Biosensors and Bioelectronics 101 (2018) 14–20

Contents lists available at ScienceDirect

Biosensors and Bioelectronics

journal homepage: www.elsevier.com/locate/bios

Multiple signal-amplification via Ag and TiO_2 decorated 3D nitrogen doped graphene hydrogel for fabricating sensitive label-free photoelectrochemical thrombin aptasensor

Nan Hao, Rong Hua, Saibo Chen, Ying Zhang, Zhou Zhou, Jing Qian, Qian Liu, Kun Wang*

Key Laboratory of Modern Agriculture Equipment and Technology, School of Chemistry and Chemical Engineering, Jiangsu University, Zhenjiang 212013, PR China

ARTICLE INFO

Keywords:
Graphene hydrogel
TiO_2
Nitrogen doping
Photoelectrochemical sensing

ABSTRACT

In this study, Ag/TiO_2/3D nitrogen doped graphene hydrogel (3DNGH) was prepared for the first time and the photocurrent intensity of this material was greatly enhanced, which was attributed to the multiple enhancements accomplished in one step. The porous structure of 3DNGH could provide an exceptionally large accessible surface area, which was beneficial for the anchoring of Ag and TiO_2 nanoparticles. The introduction of nitrogen doped graphene and metal nanoparticles was capable to facilitate the charge separation efficiency and accelerate the transfer rate of the photogenerated electron-hole pairs. Then the photoelectrochemical performance was further amplified by the localized surface plasmon resonance of Ag nanoparticles. On the basis of excellent PEC properties of Ag/TiO_2/3DNGH, a sensitive label-free PEC sensor has been established for the determination of thrombin successfully. This proposed PEC biosensor exhibited good PEC performances with a wide linear in the range from 0.01 p.M. to 10 p.M. as well as a relative low detection limit of 3 fM (S/N = 3), indicating that Ag/TiO_2/3DNGH would serve as a promising photoactive material in the applications of PEC biosensors.

1. Introduction

Recently, photoelectrochemical (PEC) sensor is a novel developed and potential analytical technique, which is based on the relationship between the changes of photovoltage/photocurrent and the concentration of target analyte under light irradiation (Wang et al., 2014a; Zhang et al., 2014b). PEC sensors have attracted considerable attention owing to high sensitivity, low background current, rapid measurement speed and inexpensive platform (Freeman et al., 2013; Zhao et al., 2014; Zhou et al., 2015). It is well known that excellent photoactive materials play a crucial role in the applications of PEC sensors. As a kind of semiconductor material, TiO_2 has been attracted much attention owning to its long term stability, non-toxicity, strong oxidizing activity, and good biocompatibility (Bian et al., 2014; Liu et al., 2013). However, the low absorption efficiency in the visible light and the recombination of photogenerated electron-hole pairs seriously impede their PEC application (Fan et al., 2016a, 2016b). Consequently, significant efforts have been devoted to enhance the photoactivity of TiO_2 in the visible light region. Noble metals such as Ag, Au nanoparticles (NPs) can effectively accelerate the electron transfer and reduce the recombination rate of the photogenerated electron-hole pairs due to the localized surface plasmon resonance (LSPR) (Mubeen et al., 2011). Meanwhile, integrating graphene with TiO_2 nanoparticle was regarded as an efficient approach to improve the photoactivity performance of TiO_2 (Fan et al., 2011; Song et al., 2012).

Graphene, as a two-dimensional sp^2-hybridized carbon nanosheet, possesses a high specific surface area and high thermal conductivity (Liu et al., 2016; Wang et al., 2012). In addition, graphene has high mobility of the charge carriers, which can strongly improve the electrical conductivity of those graphene containing metal oxide nanocomposites (Liu et al., 2014; Wang et al., 2011). However, most of the composite materials with two-dimensional structure restrict the improvement of the specific surface area. Assembling graphene nanosheets into 3D architectures has been considered as one of the most promising methods to solve the above issues. Compared with 2D graphene, the three-dimensional (3D) graphene structure not only possesses the peculiar properties of individual graphene building blocks, but also has an exceptionally large accessible surface area to increase active sites for immobilizing nanomaterials, which has been widely applied in photocatalysis (Jiao et al., 2015). gas sensing (Guo et al., 2016), supercapacitors (Jiang et al., 2016b) and other electrochemical applications (Li et al., 2017). For example, Wang et al fabricated Co_3O_4 nanoflower (NF) /graphene oxide hydrogels hybrid structures, the hydrogel provided the large surface area that could disperse the Co_3O_4

* Corresponding author.
E-mail address: wangkun@ujs.edu.cn (K. Wang).

http://dx.doi.org/10.1016/j.bios.2017.10.014
Received 27 June 2017; Received in revised form 25 September 2017; Accepted 7 October 2017
Available online 08 October 2017
0956-5663/

without agglomeration and facilitated the glucose redox reaction on Co_3O_4 NFs. 3D-graphene aerogels (GAs) could better adsorb organic pollutants and could provide multidimensional electron transport pathways (Le Thuy et al., 2016). Meanwhile, nitrogen doping can further facilitate charge transfer with adjacent carbon atoms and suppress the electrons and holes recombination (Liu et al., 2015; Meng et al., 2013). Thus, it is meaningful to explore the integration of Ag, TiO_2 and 3D nitrogen doping graphene hydrogel (3DNGH) and studied the performances of Ag/TiO_2/3DNGH.

Thrombin, as one of the immanent proteins in human, can convert soluble fibrinogen into insoluble fibrin. Over-expression or activity imbalance of thrombin can generate many diseases such as thrombosis, inflammation, atherosclerosis, and hemophilia (Li et al., 2014b, 2010). Therefore, it is very valuable to accurately detect thrombin concentration in the disease diagnosis and drug discovery. Several studies have reported the fabrication of PEC thrombin aptasensor with high PEC active nanocomposites, such as g-C_3N_4/TiO_2 (Fan et al., 2016a, 2016b) and graphene-CdS (Li et al., 2015a, 2015b), etc. To further improve the sensitivity, we studied the synthesis of Ag/TiO_2/3DNGH via a simple one-pot hydrothermal process for the first time and the photocurrent intensity was greatly enhanced due to the multiple signal amplification. The porous structure of 3DNGH could provide an exceptionally large accessible surface area for the anchoring of Ag and TiO_2. The introduction of nitrogen doped graphene and metal nanoparticles was capable to facilitate the charge separation efficiency and accelerate the transfer rate of the electron-hole pairs. Then the photoelectrochemical performance was further amplified by the LSPR of AgNPs. On the basis of excellent PEC properties of Ag/TiO_2/3DNGH, a sensitive label-free PEC sensor has been established for the determination of thrombin successfully with a wide linear in the range from 0.01 p.M. to 10 p.M. as well as a relative low detection limit of 3 fM (S/N = 3, $R^2 = 0.98$), indicating that Ag/TiO_2/3DNGH would be a promising material for PEC sensing.

2. Experimental section

2.1. Reagents and chemicals

Graphite was purchased from Qingdao Tianhe Graphite Co., Ltd. Graphene oxide (GO) was synthesized according to a modified Hummers method.[1] $Ti(SO_4)_2$, glycine(Gly), $AgNO_3$ and N, N-dimethylformamide (DMF) were obtained from Sinopharm Chemical Reagent Co., Ltd. Glucose oxidase (GOD), acetylcholine esterase (AchE), Lysozyme and Thrombin were purchased from Sigma-Aldrich Chemical Co. (St. Louis, MO, USA). Thrombin aptamer (TBA): 5′-SH-$(CH_2)_{10}$-GGT TGG TGT GGT TGG-3′was synthesized and purified by Sangon Biological Engineering Technology & Co. Ltd. (Shanghai, China) and Bovine serum albumin (BSA) was purchased from Aladdin Chemistry Co., Ltd. 0.1 M PBS (pH 7.4) was prepared by mixing stock standard solutions of NaH_2PO_4 and Na_2HPO_4. Double-distilled water was used throughout the study. Other reagents were of analytical grade and used as received without further purification.

2.2. Apparatus

The crystal structure identification was determined by X-ray diffraction (XRD) using a Bruker D8 diffractometer with high-intensity Cu Kα radiation (l = 1.54 Å) in the range of 2θ = 10-80º. The transmission electron microscopy (TEM) image was taken with a JEOL2100 transmission electron microscopy (JEOL, Japan) and scanning electron microscopy was conducted using (SEM, JEOL JSM-6700, Japan) equipped with an energy-dispersive spectroscopy (EDS, Oxford Inca Energy 400, UK). Raman spectra were surveyed with (RM 2000 microscopic confocal Raman spectrometer, England). X-ray photoelectron spectroscopy was performed on X-ray photoelectron spectrometer (PHI 5000 VersaProbe, Japan). All PEC measurements were performed with a CHI660B electrochemical analyzer (Chen Hua Instruments, Shanghai, China) and carried out in 0.1 M phosphate buffer (PBS) at 0 V and a 250 W Xe lamp (CHFXM 35-500W, Beijing Chang tuo) was utilized as the irradiation source (passing through a 400 nm UV-cut filter). Electrochemical impedance spectra (EIS) were conducted using ZENNIUM electrochemical workstation and the reference electrode (saturated calomel electrode), the counter electrode (platinum electrode), and the working electrode were connected respectively. Then, the working electrode, the reference electrode and the counter electrode were immersed in 0.1 M KCl solution containing 5 mM $Fe(CN)_6^{3-/4-}$ with the frequency range from 0.01 Hz to 10 kHz at 0.23 V, and the amplitude of the applied sine wave potential in each case was 5 mV.

2.3. Preparation of Ag/TiO_2/3DNGH hydrogels

Ag/TiO_2/3DNGH hydrogels were synthesized by one-step hydrothermal treatment. Typically, 5 mL (4 mg/mL) graphene oxide (GO) solution was dispersed in 5 mL water with sonication for 1 h to obtain a homogeneous suspension. Then, 100 mg Glycine (Gly), 0.24 g $Ti(SO_4)_2$ and 30 mg silver nitrate were added into the above GO solution (The silver content was optimized as presented in Fig. S1A.). After sonicated for 1 h, the above suspension was transferred into a Teflon-sealed autoclave and heated at 180 °C for 12 h. The synthetic hydrogels (Ag/TiO_2/3DNGH) were washed with water and then stored in pure water. For comparison, TiO_2/3DNGH was also prepared under the same condition without $AgNO_3$. And the Ag/TiO_2/graphene hydrogels (Ag/TiO_2/3DGH) were synthesized without Gly. Finally, the hydrogels samples were freeze dried at −37 °C for 2 days. The pure TiO_2 and the Ag/TiO_2/NG nitrogen doped graphene were synthesized by using the method as described in earlier report (Jiang et al., 2016a).

2.4. Fabrication of the modified electrodes

Primarily, the ITO electrodes were obtained by a series of pretreatment according to previous reports (Jiang et al., 2016a). 2 mg mL^{-1} Ag/TiO_2/3DNGH suspension was prepared by dispersing 2.0 mg of Ag/TiO_2/3DNGH in 1.0 mL of DMF with ultrasonic agitation. Then, 20 μL of suspension obtained was dropped onto ITO slice with a fixed area of 0.5 cm^2 and dried under an infrared lamp. After that, in order to better fix the material and prevent the material from falling off during the experiment, 10 μL of chitosan solution was covered on it, and also dried in ambient air to obtain modified ITO (Ag/TiO_2/3DNGH/ITO) electrode. For comparison, TiO_2/ITO, TiO_2/3DNGH and Ag/TiO_2/3DGH modified ITO electrodes were obtained with above similar procedure.

2.5. Fabrication of the aptasensor for thrombin

The PEC aptasensor fabrication process was illustrated in Scheme 1 as follows: 10 μL of 5 μmol L^{-1} thrombin aptamer (TBA) solution (The optimized concentration of aptamer as shown in Fig. S1B.) was dropped onto the surface of Ag/TiO_2/3DNGH modified ITO electrode and then allowed to react at 4 °C for 12 h to ensure that aptamer was successfully immobilized on Ag/TiO_2/3DNGH/ITO via the covalent bond formed between sulfydryl group of TBA and Ag. After the reaction completed, the electrodes were rinsed with PBS to remove physically absorption. Subsequently, the electrodes were covered with 10 μL of 1% bovine serum albumin (BSA) for 1 h at 4 °C to deactivate the unreacted active sites on the electrode surface and then washed thoroughly. Then, the as-prepared aptamer Ag/TiO_2/3DNGH/ITO electrodes were incubated in 10 μL of 0.1 M PBS containing different concentrations of thrombin solutions for 40 min at 37 °C (see the Supplementary material; Fig. S1C and Fig. S1D). And thrombin was immobilized on the modified electrode surface by the specific recognition affinity reaction between TBA and thrombin, followed by thoroughly rinsing with PBS. Finally, the TBA aptamer modified Ag/TiO_2/3DNGH electrodes were successfully

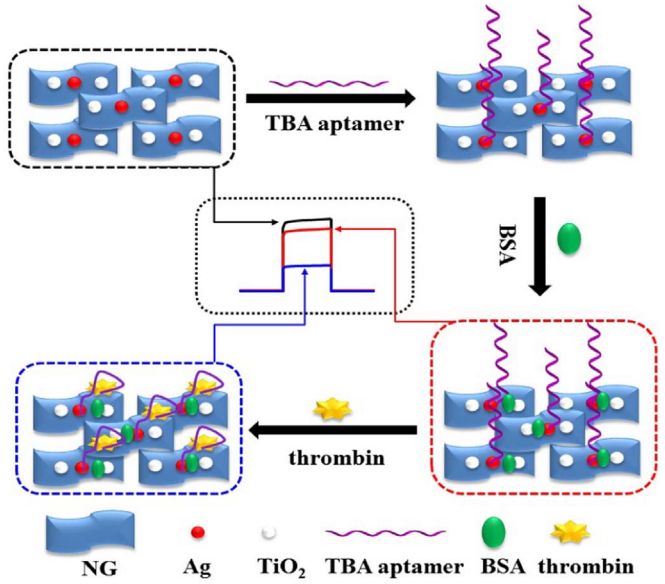

Scheme 1. The schematic diagram of the as-fabricated Ag/TiO_2/3DNGH aptasensor for detecting thrombin.

developed and used for the detection of thrombin.

3. Results and discussion

3.1. Characterization of the samples

The morphological information of the as-synthesized Ag/TiO_2/3DNGH was detected by the field emission SEM and the TEM. SEM image of Ag/TiO_2/3DNGH was shown in Fig. 1A and the 3D internal porous structure could clearly be found. The as-prepared Ag/TiO_2/3DNGH material was further investigated by TEM characterization. Fig. 1B indicated Ag and TiO_2 nanoparticles were anchored onto 3DNGH surface. The diameters of these particle were around 10–25 nm and Ag and TiO_2 could be clearly distinguished from different contrasts. As shown in the inset, it was apparent that Ag had a higher contrast.

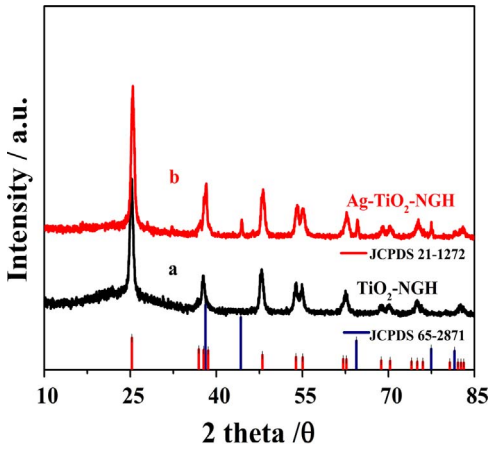

Fig. 2. XRD patterns of the TiO_2-3DNGH (a), Ag/TiO_2/3DNGH (b).

The resulting demonstrated that the successful preparation of Ag/TiO_2/3DNGH. Meanwhile, elemental mapping images (EMIs) revealed the existence of Ag, Ti, N and C elements in the Fig. 1C-F, which were consistent with XPS characterization.

The XRD patterns of as-prepared TiO_2/3DNGH (curve a), Ag/TiO_2/3DNGH (curve b) were shown in Fig. 2. The distinct diffraction peaks (2θ) at 25.3°, 37.8°, 48.1°, 53.9°, 55.1°,62.7°, 68.8°, 70.3°, 75.0° and 82.7° were attributed to the (101), (004), (200), (105), (211), (204), (116), (220), (215) and (224) crystal planes of TiO_2 (JCPDS No. 21-1272) (Wang et al., 2014b). In the patterns of Ag/TiO_2/3DNGH (curve b), the peaks at 38.1°, 44.3°, 64.5° and 77.4° could be clearly observed, which were assigned to the (111), (200), (220) and (311) crystal planes of face centered cubic Ag^0 (JCPDS No. 65-2871) (Fan et al., 2015; Wen et al., 2011), which proved the successful reduction of $AgNO_3$ under the hydrothermal. Moreover, no impurity peaks were observed in the TiO_2/3DNGH and Ag/TiO_2/3DNGH, indicating that the TiO_2 and Ag nanocrystals exhibited high crystalline quality. Simultaneously, the digital photograph of Ag/TiO_2/3DNGH was provided in Fig. S2. It was clearly seen that Ag/TiO_2/3DNGH had the complete hydrogel configuration. These results proved the successful fabrication of the Ag/TiO_2/3DNGH under proper conditions.

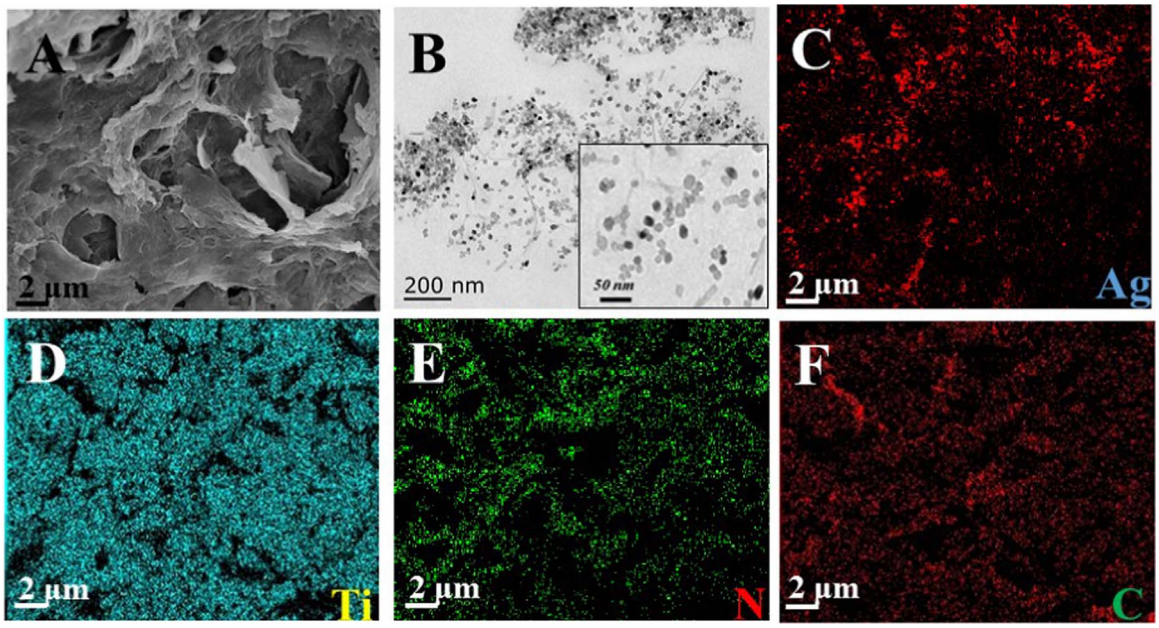

Fig. 1. (A) SEM image and (B) TEM image of Ag/TiO_2/3DNGH. Inset: high-resolution image of Ag/TiO_2/3DNGH. Elemental mapping images (EMIs) of (C) Ag, (D) Ti, (E) N, (F) C of the samples.

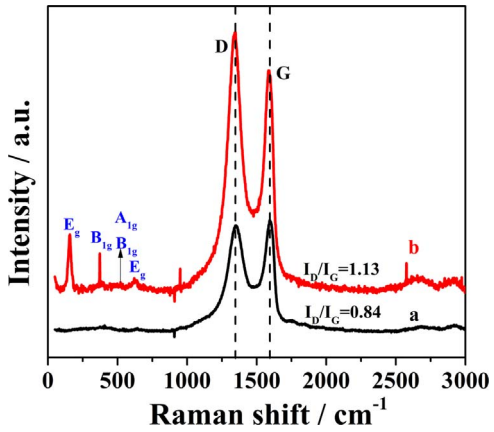

Fig. 3. Raman spectra of the TiO_2/3DNGH (a), Ag/TiO_2/3DNGH (b).

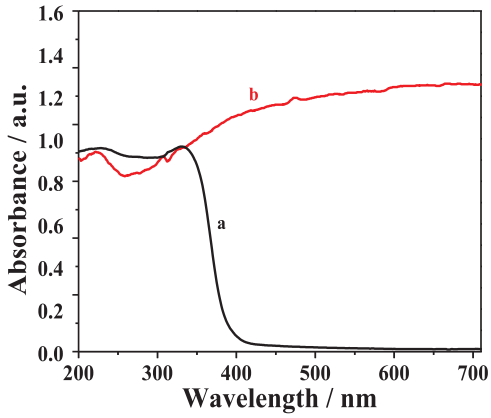

Fig. 4. UV–visible absorption spectra of (a) TiO2, (b) Ag-TiO2/3DNGH.

Raman spectroscopy was an effective tool to characterize the structural properties of graphene-based materials. The typical Raman spectras of the GO and Ag/TiO_2/3DNGH were displayed in Fig. 3. The Raman spectrum of GO (curve a) showed D and G bands at 1351 and 1593 cm^{-1}, respectively. The D band confirmed the existence of some defects within the graphene sheets, while the G band could be attributed to the result of the first order scattering of the E_{2g} mode of sp^2 carbon domains (Ji et al., 2014; Yang et al., 2015). For Ag/TiO_2/3DNGH (curve b), four distinct Raman peaks of anatase TiO_2 could be observed at 145 (E_g), 399 (B_{1g}), 519 ($A_{1g}+B_{1g}$) and 639 cm^{-1} (E_g), further proving that all the combinations of synthesized samples resulted in anatase phase (Sim et al., 2014; Zhang et al., 2014a). In Raman spectra, the intensity ratio of D and G band (I_D/I_G) was a measure of disorder degree of the sp^2 domains. The I_D/I_G value of Ag/TiO_2/3DNGH (1.13) was much greater than that of GO (0.84). Compared with TiO_2/3DNGH nanocomposites, the crystal defects of Ag/TiO_2/3DNGH nanocomposites increase due to the incorporation of Ag. In this case, the intensity of the D peak is enhanced in the Raman spectrum, resulting in an increase in the ratio of I_D / I_G.

The surface compositions and elemental chemical states of the Ag/TiO_2/3DNGH were further investigated by X-ray photoelectron spectroscopy (XPS). As could be seen from Fig. S3A, the survey spectrum of Ag/TiO_2/3DNGH showed five predominant peaks at 284.6, 367.6, 401.6, 458.5 and 529.7 eV which were corresponded to the C 1s, Ag 3d, N1s, Ti 2p and O 1s, respectively. Fig. S3B showed two strong peaks at 458.5 and 464.4 eV and they were assigned to Ti $2p_{3/2}$ and Ti $2p_{1/2}$ (Wei et al., 2014), respectively, which confirmed that in the nanocomposites Ti existed mainly in the Ti^{4+} state. As shown in Fig. S3C, a representative Ag 3d core level XPS spectrum with two peaks located at 367.6 and 373.5 eV could be attributed to Ag $3d_{5/2}$ and Ag $3d_{3/2}$ which was another evidence of the reduction of $AgNO_3$ by the solvothermal method to produce metallic silver (Xiao, 2012). Fig. S3D revealed the expanded XPS spectrum of the C1s peaks at 284.5(pink line), 285.9(green line), 286.5(navy line) and 289.0 eV (purple line), which could be assigned to C-C, C-N, C-O (epoxyl and hydroxyl) and O-C=O, respectively. All the observations confirmed the existence of Ag and TiO_2 in the 3DNGH and the nanocomposites of Ag/TiO_2/3DNGH was successfully formed.

3.2. Photoelectrochemical measurements

The UV–vis diffuse reflectance absorption spectra of TiO_2 and Ag/TiO_2/3DNGH samples were measured and presented in Fig. 4. The spectra of Ag/TiO_2/3DNGH showed greater absorption than that of pure TiO_2 in the visible range due to the presence of NGR and Ag NPs. Moreover, the Ag/TiO_2/3DNGH showed a small absorption peak at approximately 475 nm (Jiang et al., 2015), which can be attributed to the surface plasmon resonance of Ag nanoparticles. This result further showed the presence of metallic Ag NPs on the surface of Ag/TiO_2/3DNGH.

The PEC behaviors of different modified electrodes were investigated in 0.1 M PBS (pH 7.4) under visible light irradiation (Fig. 5A). The photocurrent with a value of 4 nA was observed for pristine TiO_2 modified ITO (curve a). Then the photocurrent intensity of the TiO_2/3DNGH modified electrode was remarkably enhanced to 2.5 μA (curve b). It could be explained that the 3DNGH effectively stored the photogenerated electrons and enhanced the electron-hole pair charge separation, reducing the recombination rate of photogenerated electrons and holes and resulting the increased photocurrent intensity (Jiang et al., 2015). After the introduction of Ag (curve c), the photocurrent intensity increased to 4.2 μA, which could be attributed that the addition of Ag possessed an excellent ability to accelerate electrons transfer and the existence of localized surface plasmon resonance (Wen et al., 2011). Under light irradiation, electrons would be enriched on the surface of Ag and transferred to TiO_2 subsequently (Fan et al., 2015). Noteworthy, the photocurrent intensity of Ag/TiO_2/3DNGH was nearly 3.1 fold enhancement than Ag/TiO_2/ nitrogen doped graphene (NG) nanocomposites. The reason might be attributed to the 3D internal porous structure of Ag/TiO_2/3DNGH, which could provide a large surface area for the anchoring of Ag and TiO_2 nanoparticles and result in the enhanced PEC performances (Nhi Sa et al., 2016). In order to show the positive effect of N-doping in the PEC response, the photocurrent response Ag/TiO_2/3DGH and Ag/TiO_2/3DNGH were provided in Fig. 5B. After the introduction of N chemical element, the Ag/TiO_2/3DNGH modified electrode exhibited the stronger photocurrent (curve a) than Ag/TiO_2/3DGH (curve b) under light irradiation, which might be attributed to the introduction of nitrogen atoms was beneficial to improve the photoinduced carriers separation efficiency and suppress recombination of the electron-holes (Jiang et al., 2014).

3.3. Fabrication and characterization of the PEC aptasensor

To understand the PEC sensing mechanism of the proposed sensor, time-dependent photocurrent responses of the PEC aptasensor in different stages were presented in Fig. 6A. As shown in Fig. 6A (curve a), Ag/TiO_2/3DNGH possessed a good photoelectrical property and exhibited a powerful photocurrent of 4.2 μA, which confirmed that the enhanced lifetime of the excitons and efficient charge separation. With the modification of thrombin aptamer onto the Ag/TiO_2/3DNGH (curve b), the photocurrent decreased due to the presence of aptamer molecules which enhanced the steric hindrance of the electrode interface and block the electron transfer (Yan et al., 2015). After the aptasensor having specific reaction with 0.5 p.M. target analyte thrombin, the photocurrent response drastically decreased (curve c). The photocurrent decrease could be explained by the immobilized

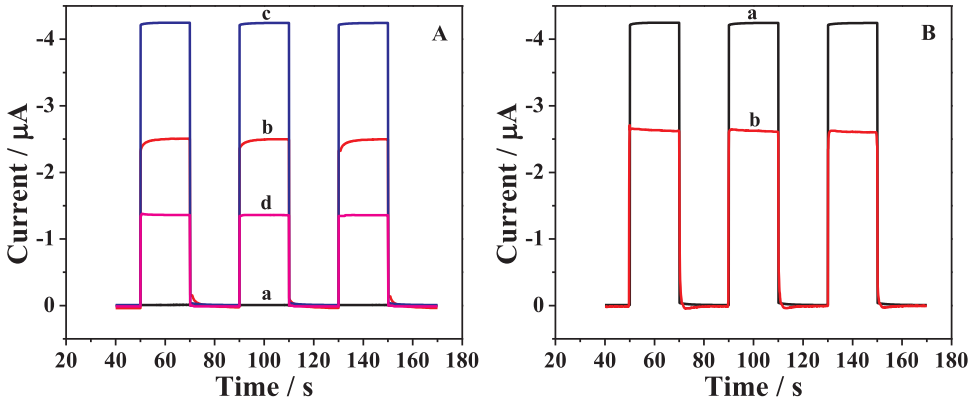

Fig. 5. (A) Photocurrent responses of pristine TiO_2 (curve a), TiO_2/3DNGH (curve b), Ag/TiO_2/3DNGH (curve c) and Ag/TiO_2/NG nanocomposites (curve d). (B) Photocurrent response of Ag/TiO_2/3DNGH (curve a) and Ag/TiO_2/3DGH (curve b).

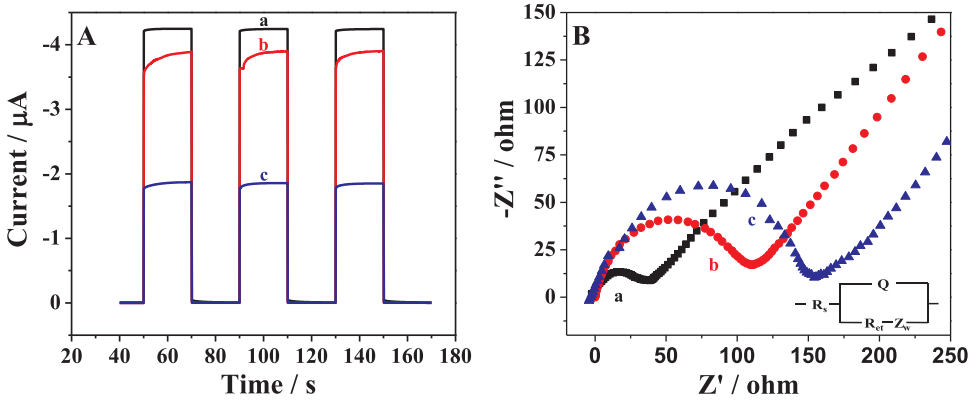

Fig. 6. PEC (A) and EIS (B) characterization of the aptasensor fabrication process: Ag/TiO_2/3DNGH/ITO (curve a), aptamer Ag/TiO_2/3DNGH modified ITO (curve b) and thrombin interact with the aptamer Ag/TiO_2/3DNGH modified ITO (curve c).

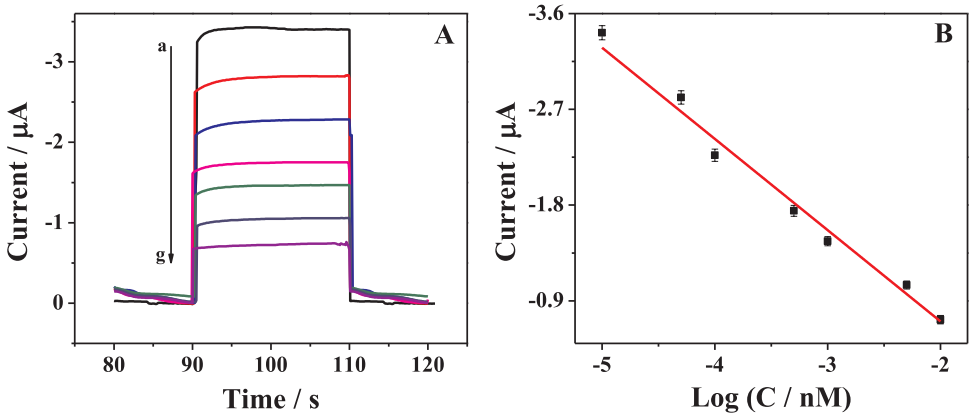

Fig. 7. (A) Time-based photocurrent response (a) 1 × 10^{-5} nM, (b) 5 × 10^{-5} nM, (c) 1 × 10^{-4} nM, (d) 5 × 10^{-4} nM, (e) 1 × 10^{-3} nM, (f) 5 × 10^{-3} nM, (g) 1 × 10^{-2} nM and (B) logarithmic calibration curve for PEC aptasensor for the detection of different concentrations of thrombin.

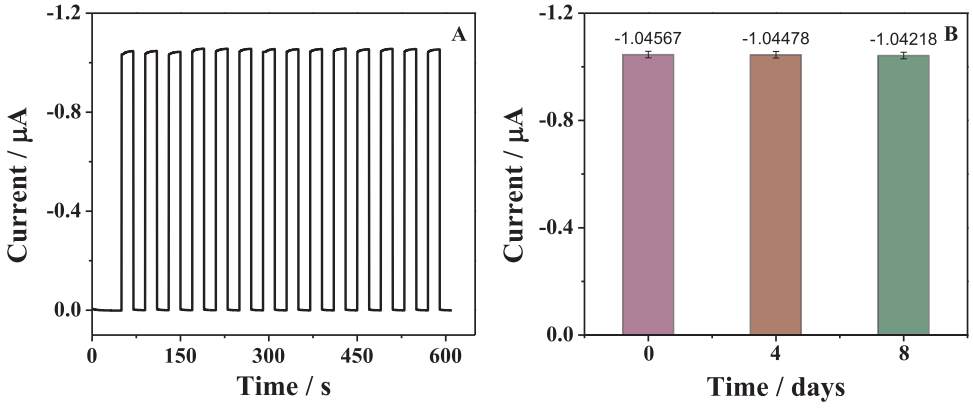

Fig. 8. (A) Photocurrent response of the PEC aptasensor under several on/off irradiation cycles for 610 s (B) Photocurrent response of the PEC aptasensor after 0 day, 4 days, and 8 days (n = 5).

biomacromolecule hindered the electron-transfer (Fan et al., 2013).

To evaluate the electron transfer ability of the stepwise assembly process of the aptasensor, EIS was performed using $[Fe(CN)_6]^{3-/4-}$ as a redox probe (Fig. 6B). The equivalent circuit (Fig. 6B, inset) used for fitting the impedance data, where R_s, R_{et}, Z_w and Q represented electrolyte solution resistance, electron transfer resistance, warburg impedance and constant phase elements, respectively. As could be seen, the R_{et} of Ag/TiO_2/3DNGH modified electrode (curve a) had a R_{et} of 36 Ω, implying NGH and Ag could effectively speed up the electron transfer. When thrombin aptamer was modified on the electrode surface, the R_{et} value increased to 100 Ω (curve b), which could be attributed to negatively charged backbones of aptamer, thus hindering the transfer of electrons. It indicated the thrombin aptamer loaded on surface of the electrode successfully. In the presence of 0.5 p.M. target analyte thrombin, owing to the thrombin by captured aptamer covered onto the surface of the electrode, further hindering the electron transfer, the electron transfer resistance became larger (curve c) than before (curve b).

3.4. Photoelectrochemical detection of thrombin

Based on the excellent photoelectric properties of Ag/TiO_2/3DNGH, the developed aptamer/Ag/TiO_2/3DNGH/ITO electrode was applied to the quantitative determination of thrombin. Fig. 7A exhibited the photocurrent response of Ag/TiO_2/3DNGH modified electrodes with different concentrations of thrombin under visible light illumination. As shown in Fig. 7B, the photocurrent decreased gradually with increasing concentrations of thrombin and the photocurrent intensity was linear with the logarithm of thrombin concentrations in the range of 0.01 p.M. to 10 p.M. as well as a low detection limit of 3 fM (S/N = 3). The achieved limit of detection in our work was satisfying compared with those published reports, which were summarized in Table S1 (Li et al., 2014a, 2015a, 2015b; Liang et al., 2011; Sui et al., 2016; Yue et al., 2014). We also tested the performance of this sensor in human serum by the standard addition method (Table S2). And the recoveries were in the range of 96.0–102.5%. These results indicated that the Ag/TiO_2/3DNGH could be used as a novel material for PEC sensing.

3.5. Selectivity of the biosensor

The influence of 100 p.M. of different proteins in the serum, including myoglobin, C-reactive protein (CRP) and troponin, on the photocurrent intensity of developed electrodes was examined (Fig. S4). It had no influence on the PEC sensing although the 10-fold of the interference compared with that of the sensor incubated with thrombin, which disclosed that the fabricated PEC biosensor showed good selectivity for thrombin because of the specific recognition between aptamer and thrombin.

3.6. Stability and reproducibility of the PEC aptasensor

In order to research the stability of the aptasensor, the photocurrent response of the PEC aptasensor were recorded as the excitation light was turned on and off continuously (Fig. 8A). It presented obviously that the PEC intensity of aptamer/Ag-TiO_2/3DNG was very stable over 610 s, which indicated that the aptamer molecules would not fall off easily from the ITO surface and the aptasensor itself had long-time stability. In addition, the reproducibility of the aptasensor was evaluated by testing a series of five electrodes prepared in the same way. The relevant results provided in Fig. 8B, which indicated that the average photocurrent intensity of the aptasensor for the detection of thrombin. The relative standard deviation (RSD) was recorded as 4.4%, indicating that the proposed aptasensor has a remarkable reproducibility for the detection of thrombin.

3.7. Real sample analysis

To further demonstrate the practicality of the proposed method, the recovery test was studied by adding different concentrations of thrombin into serum samples. The results were summarized in Table S2, and the recovery rate of this method ranged from 96.0% to 102.5%, which indicated that the proposed method was stable and could be applied for analysis of real samples.

4. Conclusion

In summary, a label-free photoelectrochemical aptasensor for ultrasensitive detection of thrombin was developed based on Ag/TiO_2/3DNGH by one step hydrothermal method. With the synergy of the porous structure, the localized surface plasmon resonance, the improved separation efficiency and transfer rate of the photoinduced electron-hole pairs, the as-prepared Ag/TiO_2/3DNGH showed outstanding photoelectrochemical performances after multiple enhancements. The photocurrent intensity was greatly enhanced. Based on this nanocomposite, a sensitive PEC sensor was developed, which exhibited a broader linear range from 0.01 p.M. to 10 p.M. as well as a detection limit down to 3 fM, indicating Ag/TiO_2/3DNGH would be potentially attractive for the PEC related applications.

Acknowledgments

This work was supported by National Natural Science Foundation of China (Nos. 21505055, 21675066 and 21375050), Natural Science Foundation of Jiangsu Province (No. BK20150486), Foundation of Jiangsu University (15JDG145), Project Funded by the Priority Academic Program Development of Jiangsu Higher Education Institutions (No. PAPD-2014-37) and Qing Lan Project. Jiangsu Province Science and Technology Support Program (Industry) project (BE2014510). State Key Laboratory of Analytical Chemistry for Life Science (SKLACLS1504).

Appendix A. Supporting information

Supplementary data associated with this article can be found in the online version at http://dx.doi.org/10.1016/j.bios.2017.10.014.

References

Bian, Z., Tachikawa, T., Zhang, P., Fujitsuka, M., Majima, T., 2014. J. Am. Chem. Soc. 136 (1), 458–465.
Fan, D., Guo, C., Ma, H., Zhao, D., Li, Y., Wu, D., Wei, Q., 2016b. Biosens. Bioelectron. 75, 116–122.
Fan, W., Lai, Q., Zhang, Q., Wang, Y., 2011. J. Phys. Chem. C 115 (21), 10694–10701.
Fan, Y., Ma, W., Han, D., Gan, S., Dong, X., Niu, L., 2015. Adv. Mater. 27 (25), 3767–3773.
Fan, W., Yu, X., Lu, H.C., Bai, H., Zhang, C., Shi, W., 2016a. Appl. Catal., B 181, 7–15.
Fan, L., Zhao, G., Shi, H., Liu, M., Li, Z., 2013. Biosens. Bioelectron. 43, 12–18.
Freeman, R., Girsh, J., Willner, I., 2013. ACS Appl. Mater. Interfaces 5 (8), 2815–2834.
Guo, D., Cai, P., Sun, J., He, W., Wu, X., Zhang, T., Wang, X., Zhang, X., 2016. Carbon 99, 571–578.
Ji, Z., Shen, X., Yang, J., Zhu, G., Chen, K., 2014. Appl. Catal. B 144, 454–461.
Jiang, D., Du, X., Liu, Q., Zhou, L., Qian, J., Wang, K., 2015. ACS Appl. Mater. Interfaces 7 (5), 3093–3100.
Jiang, D., Du, X., Chen, D., Zhou, L., Chen, W., Li, Y., Hao, N., Qian, J., Liu, Q., Wang, K., 2016a. Biosens. Bioelectron. 83, 149–155.
Jiang, L., Lin, B., Li, X., Song, X., Xia, H., Li, L., Zeng, H., 2016b. ACS Appl. Mater. Interfaces 8 (4), 2680–2687.
Jiang, D., Liu, Q., Wang, K., Qian, J., Dong, X., Yang, Z., Du, X., Qiu, B., 2014. Biosens. Bioelectron. 54, 273–278.
Jiao, T., Zhao, H., Zhou, J., Zhang, Q., Luo, X., Hu, J., Peng, Q., Yan, X., 2015. ACS Sustainable Chem. Eng. 3 (12), 3130–3139.
Le Thuy, H., Chung, J.S., Hur, S.H., 2016. Sens. Actuators B 223, 76–82.
Li, J., Li, W., Qiang, W., Wang, X., Li, H., Xu, D., 2014a. Anal. Chim. Acta 807, 120–125.
Li, L., Lin, H., Lei, C., Nie, Z., Huang, Y., Yao, S., 2014b. Biosens. Bioelectron. 54, 42–47.
Li, L., Zhao, H., Chen, Z., Mu, X., Guo, L., 2010. Anal. Bioanal. Chem. 398 (1), 563–570.
Li, H., Zhu, X., Sitinamaluwa, H., Wasalathilake, K., Xu, L., Zhang, S., Yan, C., 2017. J. Alloy. Compd. 714, 425–432.

Li, S., Zhu, W., Xue, Y., Liu, S., 2015a. Biosens. Bioelectron. 64, 611–617.
Li, S., Zhu, W., Xue, Y., Liu, S., 2015b. Biosens. Bioelectron. 64, 611–617.
Liang, G., Cai, S., Zhang, P., Peng, Y., Chen, H., Zhang, S., Kong, J., 2011. Anal. Chim. Acta 689 (2), 243–249.
Liu, C., Tang, J., Chen, H.M., Liu, B., Yang, P., 2013. Nano Lett. 13 (6), 2989–2992.
Liu, F., Zhang, Y., Yu, J., Wang, S., Ge, S., Song, X., 2014. Biosens. Bioelectron. 51, 413–420.
Liu, J., Cui, M., Niu, L., Zhou, H., Zhang, S., 2016. Chem. Eur. J. 22 (50), 18001–18008.
Liu, Y., Yan, K., Okoth, O.K., Zhang, J., 2015. Biosens. Bioelectron. 74, 1016–1021.
Meng, F., Li, J., Cushing, S.K., Zhi, M., Wu, N., 2013. J. Am. Chem. Soc. 135 (28), 10286–10289.
Mubeen, S., Hernandez-Sosa, G., Moses, D., Lee, J., Moskovits, M., 2011. Nano Lett. 11 (12), 5548–5552.
Nhi Sa, N., Das, G., Yoon, H.H., 2016. Biosens. Bioelectron. 77, 372–377.
Sim, L.C., Leong, K.H., Ibrahim, S., Saravanan, P., 2014. J. Mater. Chem. A 2 (15), 5315–5322.
Song, P., Zhang, X., Sun, M., Cui, X., Lin, Y., 2012. Nanoscale 4 (5), 1800–1804.
Sui, N., Wang, L., Xie, F., Liu, F., Xiao, H., Liu, M., Yu, W.W., 2016. Microchim. Acta 183 (5), 1563–1570.
Wang, G.L., Liu, K.L., Dong, Y.M., Wu, X.M., Li, Z.J., Zhang, C., 2014a. Biosens. Bioelectron. 62, 66–72.
Wang, H., Maiyalagan, T., Wang, X., 2012. ACS Catal. 2 (5), 781–794.
Wang, K., Li, H.N., Wu, J., Ju, C., Yan, J.J., Liu, Q., Qiu, B., 2011. Analyst 136 (16), 3349–3354.
Wang, L., Ma, W., Gan, S., Han, D., Zhang, Q., Niu, L., 2014b. Anal. Chem. 86 (20), 10171–10178.
Wei, X.X., Chen, C.M., Guo, S.Q., Guo, F., Li, X.M., Wang, X.X., Cui, H.T., Zhao, L.F., Li, W., 2014. J. Mater. Chem. A 2 (13), 4667–4675.
Wen, Y., Ding, H., Shan, Y., 2011. Nanoscale 3 (10), 4411–4417.
Xiao, F.X., 2012. ACS Appl. Mater. Interfaces 4 (12), 7055–7063.
Yan, K., Liu, Y., Yang, Y., Zhang, J., 2015. Anal. Chem. 87 (24), 12215–12220.
Yang, B., Zuo, X., Chen, P., Zhou, L., Yang, X., Zhang, H., Li, G., Wu, M., Ma, Y., Jin, S., Chen, X., 2015. ACS Appl. Mater. Interfaces 7 (1), 137–143.
Yue, Q., Shen, T., Wang, L., Xu, S., Li, H., Xue, Q., Zhang, Y., Gu, X., Zhang, S., Liu, J., 2014. Biosens. Bioelectron. 56, 231–236.
Zhang, X., Liu, M., Mao, Y., Xu, Y., Niu, S., 2014b. Biosens. Bioelectron. 59, 21–27.
Zhang, J., Xiao, F.-X., Xiao, G., Liu, B., 2014a. Nanoscale 6 (19), 11293–11302.
Zhao, W.W., Xu, J.J., Chen, H.Y., 2014. Chem. Rev. 114 (15), 7421–7441.
Zhou, H., Liu, J., Zhang, S., 2015. TrAC Trends Anal. Chem. 67, 56–73.